

## Article

# Latex-Based Membrane for Oily Wastewater Filtration: Study on the Sulfur Concentration Effect

Khaled Abuhasel <sup>1</sup> , Yong Tzyy Jeng <sup>2</sup>, Yamuna Munusamy <sup>2</sup>, Mohamed Kchaou <sup>1,\*</sup> and Mohammed Alquraish <sup>1</sup>

<sup>1</sup> Department of Mechanical Engineering, College of Engineering, University of Bisha, P.O. Box 001, Bisha 67714, Saudi Arabia; kabuhasel@ub.edu.sa (K.A.); malquraish@ub.edu.sa (M.A.)

<sup>2</sup> Department of Petrochemical Engineering, Faculty of Engineering and Green Technology, Universiti Tunku Abdul Rahman, Petaling Jaya 31900, Malaysia; yongtj@utar.edu.my (Y.T.J.); yamunam@utar.edu.my (Y.M.)

\* Correspondence: kchaou.mohamed@yahoo.fr

**Abstract:** Nitrile butadiene rubber (NBR) latex/graphene oxide (GO) membranes were fabricated through a latex compounding and curing method which is a relatively new method to produce membranes for wastewater treatment. Hence, the steps in the production of the membrane through this new approach need to be evaluated to optimize the performance of the membrane. In this paper, the effect of sulfur loading in the range of 0.5 to 1.5 parts per hundred rubber (phr) on the morphology, crosslink density, tensile properties, permeation flux and oil rejection rate performance of NBR/GO membranes was studied. The sulfur loading was found to influence the surface morphology and integrity of the membrane which in turn affects the performance of the membrane in terms of strength, water flux and rejection rate of oil. Inaccurate sulfur loading produced a membrane with micro cracks, low surface area for filtration and could not withstand the filtration pressure. In this research work, the membrane with 1.0 phr sulfur provides the highest water flux value and oil rejection rate of 834.1 L/m<sup>2</sup>·hr and 92.23%, respectively. Surface morphology of 1.0 phr sulfur-loaded membrane revealed the formation of continuous membrane with high structural integrity and with wrinkles and folded structure. Furthermore, micro cracks and a less effective surface area for filtration were observed for membranes with 0.5 and 1.5 phr sulfur loading.

**Keywords:** graphene oxide; nitrile butadiene rubber; oily wastewater; membrane filtration; sulfur



**Citation:** Abuhasel, K.; Jeng, Y.T.; Munusamy, Y.; Kchaou, M.; Alquraish, M. Latex-Based Membrane for Oily Wastewater Filtration: Study on the Sulfur Concentration Effect. *Appl. Sci.* **2021**, *11*, 1779. <https://doi.org/10.3390/app11041779>

Received: 25 January 2021

Accepted: 8 February 2021

Published: 17 February 2021

**Publisher's Note:** MDPI stays neutral with regard to jurisdictional claims in published maps and institutional affiliations.



**Copyright:** © 2021 by the authors. Licensee MDPI, Basel, Switzerland. This article is an open access article distributed under the terms and conditions of the Creative Commons Attribution (CC BY) license (<https://creativecommons.org/licenses/by/4.0/>).

## 1. Introduction

Water is the most essential substance for all living things on earth. Reliable access to clean and affordable water has become a world-wide problem due to the continuous growth in water demand [1]. In the last century, the global population quadrupled and the world water demand increased sevenfold [2]. The World Water Council also estimates that by 2030, 3.9 billion people will live in regions characterized as “water scarce” [3]. With extensive industrial development, water quality has worsened over the years. A large volume of oily wastewater has been discharged indiscriminately from oil and gas fields, food and beverage, petrochemical and metal processing industries [4]. Oily wastewater discharge can cause pollution to surface water, underground water and soil. The low molecular weight hydrocarbon and petroleum fraction can evaporate to the air and thus cause unpleasant smell and air pollution. Many countries are setting the regulatory limits on the maximum oil concentration in oily wastewater discharge to be within the range of 5–40 mg/L [5]. Thus, the treatment of oily wastewater is a crucial environmental issue. Conventional methods such as gravity separation, de-emulsification, dissolved air flotation, coagulation and flocculation were studied and used to treat the oily wastewater. However, several drawbacks such as high operation cost, ineffective rejection of smaller emulsified oil droplets with size less than 20 µm, corrosion of the equipment and recontamination were faced in these methods [6]. In this regard, the membrane-based oily wastewater cleaning

techniques such as microfiltration, nano-filtration, ultrafiltration and pervaporation are being studied extensively by researchers worldwide [7–9].

The membrane technology has large potential to remove oil–water emulsion due to its advantages in term of energy efficiency, easy process and low maintenance cost [10–12]. In spite of that, the main obstacles for the commercial use of membrane filtration in oily wastewater treatment were discovered to be low chemical resistance and the trade-off effect between permeation flux and rejection rate [13]. Yang et al. reported 98.2% rejection rate of emulsified kerosene in oily wastewater with permeation flux of only  $153.2 \text{ Lm}^{-2}\text{h}^{-1}$  [14]. Poly(vinyl chloride)-bentonite membrane could reject 97% emulsified oil from saline oily wastewater but the permeation flux was only reported as  $186 \text{ Lm}^{-2}\text{h}^{-1}$  [15]. Salahi et al. reported 97.2% removal of oil-grease content from refinery oily wastewater using polyacrylonitrile (PAN) ultrafiltration membrane with a permeation flux of  $96.2 \text{ Lm}^{-2}\text{h}^{-1}$  [16]. The high rejection rate of oil and low corresponding permeation flux were reported in many other research works as well [17,18]. Low permeation flux leads to a low volume of wastewater being treated daily, and economically this is not feasible. Moreover, current polymeric membranes possess low mechanical strength, and chemical resistance which can limit their applications in oily wastewater treatment [19].

In this research, nitrile butadiene rubber latex (NBR)/graphene oxide (GO) membrane was fabricated to overcome the tradeoff effect. NBR latex was chosen as the membrane material due to its superior chemical resistance and structural integrity [20]. The mechanical strength and chemical resistance of NBR could be tailored through the three-dimensional sulfur cross-linking network. In industry, NBR is used in a wide variety of application areas requiring oil, fuel, and chemical resistance [21]. However, the primary concern of using NBR membrane for oily wastewater filtration is its hydrophobic profile which compromises permeation flux. Thus, GO is incorporated to impart water affinity to the membrane surface [22,23]. GO was selected because it has large surface area, various oxygen-containing functional groups and exhibits good compatibility with polymers [24,25]. Moreover, in the latex compounding method, GO could be easily dispersed in the water phase of the emulsion latex and lead to homogenous filler dispersion due to its oxygen functional groups. Addition of GO into membrane matrix was reported to increase antifouling properties, separation efficiency and mechanical strength of the membrane [26,27]. Many ways to fabricate porous polymeric membranes such as stretching [28], sintering [29], phase inversion [30,31] and track etching [32] had been reported in the literature. These methods are tedious, do not promote good dispersion of GO, time-consuming and some involve large usage of solvents [33]. In this work, NBR/GO membranes are fabricated using latex compounding and curing method whereby this method requires less than two hours of membrane preparation time and does not require any solvent. The dispersion of GO in NBR is expected to be good because the compounding is done in the emulsion of latex in the aqueous phase which could facilitate the dispersion of GO containing hydrophilic functional groups.

Since latex compounding and curing is a new method in production of polymer membrane, the steps in the method need to be evaluated to optimize the performance of the membrane. In this paper, the effect of concentration of sulfur on the membrane morphology and performances are being evaluated. The relation between sulfur concentration, crosslinking level of membrane, morphology of the membrane and how it affects the water flux and rejection rate should be understood to optimize the membrane performance.

## 2. Materials and Methods

### 2.1. Materials

NBR latex with a total solid content (TSC) of 70.75% was supplied by Synthomer Sdn Bhd, Malaysia. Curing ingredients such as zinc oxide (ZnO), sulfur (S), zinc diethyl dithiocarbamate (ZDEC) and zinc mercaptobenzothiazole (ZMBT) are in aqueous paste with TSC values of 43.29%, 49.01%, 54.80%, and 55.65% respectively. All the curing ingredients were obtained from Zarm Scientific & Supplies Sdn Bhd, Malaysia. Graphene

oxide (GO) was prepared using Hummer's method [34] from graphite nanofibers supplied by Platinum Nanochem Sdn. Bhd., Malaysia.

## 2.2. Preparation of NBR/GO Membranes

GO was first mixed manually with deionized water at a ratio of 1:3 in a beaker. The paste was subjected to ultra-sonication using a probe-type QSonica ultrasonic homogenizer model Q500 supplied by Gaia Scientific Sdn. Bhd., Malaysia, to break the weak van der Waals forces that held the GO layers together. The sonification process was allowed to run for 60 min to disentangle the sheets that tended to cling together and form lumps. A paste-like mixture was obtained and ready to be used for latex compounding. Designated amounts of ingredients in parts per hundred rubber (phr) was added into a 250 mL beaker following the sequence to compound the membrane as 100 phr NBR latex, 1.0 phr KOH solution, 1.0 phr ZnO, 1.0 phr ZEDC, 0.5 phr ZMBT and 2.0 phr GO. Sulfur was added lastly to the compound and the loading of sulfur was varied as 0.5, 1.0 and 1.5 phr. The ratio of compounding ingredients is selected based on the literature review where the common loading of accelerators, activators and crosslinking agents in NBR films was adapted [35,36]. At the same time as the ingredients were added, the compound was stirred using IKA overhead stirrer model EUROSTAR Digital 20 supplied by IKA Works Asia Sdn. Bhd. at a speed of 350 rpm. After stirring for 30 min, the compound was ready for membrane casting. NBR/GO membranes with 0.05 mm thickness were then casted on the glass plate using a lab-scale membrane auto casting machine, model A4K-S564 from Autonics Sdn Bhd., Malaysia. The casting parameters were controlled at a distance of 220 mm and a forward speed of 150 rpm. The casted membranes were then cured in a conventional oven model Memmert provided by Interscience Sdn Bhd, Malaysia, at 100 °C for 2 h.

## 2.3. Characterization

Crosslink density calculation was performed through an equilibrium swelling method. NBR membrane samples with dimensions of 10 mm length, 10 mm width and 2 mm height were prepared and immersed in the beaker filled with 50 mL toluene. The beaker was kept in dark for 7 days at 25 °C. Volume fraction and crosslink density of NBR films were calculated using Equations (1) and (2), respectively [37]. The density of rubber specimens was determined by using a precision balance with a density determining kit (model ES 320A). Five tests were conducted for each NBR film and average value was calculated.

$$v_r = \frac{\frac{w_2}{\rho_2}}{\frac{w_2}{\rho_2} + \frac{(w_1 - w_2)}{\rho_1}} \quad (1)$$

where  $v_r$  is the volume fraction of rubber;  $w_1$  is the weight of swollen sample;  $w_2$  is the weight of sample after drying at 60 °C to constant weight;  $\rho_1$  is the density of the solvent (0.87 g/mol) [28];  $\rho_2$  is the density of the nitrile rubber specimen.

$$V = \left( -\frac{1}{2v_s} \right) \frac{[\ln(1 - v_r) + v_r + xv_r^2]}{\left( v_r^{\frac{1}{3}} - \frac{v_r}{2} \right)} \quad (2)$$

where  $V$  is the crosslink density;  $v_r$  is the volume fraction of rubber;  $v_s$  is the molar volume of solvent (toluene = 106.2 cm<sup>3</sup>/mol) [16];  $x$  is the rubber–solvent interaction parameter ( $x = 0.435$ ) [38].

The morphology of the membranes surface was analyzed using a field emission scanning electron microscope (FESEM), model JOEL JSM 6701F supplied by JOEL USA Inc., Peabody, MA, USA. The membranes were sputter coated with platinum particles before scanning to enhance electron charging during imaging process. The samples were then attached using carbon tape on the FESEM sample holder for imaging. Fourier Transform Infrared Spectroscopy (FTIR) analysis was carried out using Spectrum RX1 Perkin Elmer Analyzer from Perkin Elmer, USA, to determine the functional groups in the membrane.

The analysis was carried out at wavelength between 400 and 4000  $\text{cm}^{-1}$  at room temperature using attenuated total reflectance (ATR) technique. X-ray diffraction (XRD) analysis was carried out on the membranes using Siemens XRD Diffractometer Model 5000 supplied by DKSH Technology Sdn Bhd., Malaysia, which operates using nickel-filtered copper  $K\alpha$  radiation with  $\lambda = 0.154$  nm. A step scan with  $2^\circ/\text{min}$  scanning rate between the scanning angles of  $10^\circ$  and  $60^\circ$  was performed to detect the ordered structure of GO in the membrane.

#### 2.4. Performance Studies

Tensile testing on the membranes was carried out with a load setting of 450 N, an extension length of 1200 mm and a stretching speed of 100 mm/min using a light-weight tensile tester, model H10KS-0748 from Tinius Olsen. Testing Machine Company supplied by Leader Technology Scientific (M) Sdn. Bhd., Malaysia. The test was carried out in accordance with ASTM D882-10 standard. The membranes were cut into dumbbell-shaped samples with gauge length of 26 mm and neck width of 3 mm for testing. The ultimate tensile strength (UTS), E-modulus and elongation at break (EB) of the membranes were recorded from this test. For each sulfur formulation, 5 samples were tested and the average result was taken. Permeation flux test was performed at the operating pressure of 0.5 and 1.0 bar with synthetic oily wastewater by using a dead-end membrane test rig custom-made by Shxp Trading, Malaysia. Five membrane samples were used for each set of tests and the average value of permeate flux was calculated. Synthetic oily wastewater with oil content of 1000 ppm was prepared by emulsifying diesel with DI water and 0.01 wt.% of sodium dodecyl sulfate (SDS) for 30 min using a probe-type QSonica ultrasonic homogenizer model Q500 supplied by DKSH Holdings (M) Berhad, Malaysia. The oil particle size was estimated by Lighthouse liquid particle counter, model LS-20 supplied by Lighthouse Worldwide Solution (M) Sdn. Bhd., Malaysia. All droplet sizes fell within a specified range of 1.0–50  $\mu\text{m}$  with the majority of droplet sizes around 7  $\mu\text{m}$ . The permeate flux was calculated using Equation (3). The membrane used for the filtration cell was fixed to a mandatory nominal diameter of 50 mm to control the effective membrane area for permeate flux at  $1.0179 \times 10^{-3} \text{ m}^2$ . The time taken to collect 30 mL of filtrate was recorded.

$$J_p = \frac{V_p}{A \times t} \quad (3)$$

where

$J_p$ —Permeation flux,  $\frac{\text{L}}{\text{m}^2 \cdot \text{hr}}$ ;

$V_p$ —Permeate volume collected, L;

$A$ —Effective membrane area,  $\text{m}^2$ ;

$t$ —Time taken to collect the measured volume of permeate, h.

The oil rejection efficiency of the membranes was evaluated by preserving the filtrate for the chemical oxygen demand (COD) test. HACH COD vials and a HACH COD digester rack were used to digest the samples. After the digestion was completed, reading of COD was taken using HACH DR6000 UV-VIS Spectrophotometer. The oil rejection efficiency was obtained by comparing the oil content in feed synthetic oily wastewater and the filtrate COD by using Equation (4). For each set of membranes and pressures, COD test was carried out five times and average value was calculated.

$$R = \left( 1 - \frac{\text{COD}_p}{\text{COD}_f} \right) \times 100\% \quad (4)$$

where

$R$ —Oil rejection efficiency, %;

$\text{COD}_p$ —COD level in permeate, mg/L;

$\text{COD}_f$ —COD level in wastewater feed, mg/L.

### 3. Results and Discussion

#### 3.1. Characterization of the Membrane

Crosslink density of the membrane increases as the sulfur loading increases from 0.5 to 1.5 phr (Table 1). Addition of sulfur forms a three-dimensional network between NBR macromolecular chains. This network holds the chains together and prevents the chains from slipping past each other when subjected to force, thus increasing the strength of NBR [39]. Previous studies also reported that sulfur crosslinking could produce NBR films with high resistance to biodiesel [40], gasoline and oil [41]. Thus, the sulfur crosslinking introduced in the NBR membrane in this study is expected to provide the membrane with strength and chemical resistance properties. However, the effect of the sulfur loading on the morphology of the membrane has to be understood to optimize the performance of the membrane in oily wastewater filtration.

**Table 1.** Crosslink density of the membranes with different sulfur loadings.

NBR/GO with Sulfur Formulation (phr)	Crosslink Density ( $\times 10^{-4}$ mol/cm <sup>3</sup> )
0.5	4.7270 $\pm$ 0.0028
1.0	9.0754 $\pm$ 0.0025
1.5	9.6481 $\pm$ 0.0035

SEM images of all the membranes with GO exhibit a clear wrinkled and folded surface, Figure 1b,d,f compared to pure NBR membrane as shown in Figure 1a,c,e. This is due to the low-density nature of GO that causes it to migrate up towards the membrane surface during the curing period. GO sheets contains not evenly distributed oxygen functional groups which attribute to the scoring and folding effect of the GO sheet edges [42]. This deformation of GO sheets will bring about the corrugated, scrolling and wrinkle surface in the NBR matrix membrane upon casting [43]. As a result, the folds create ridges and grooves which increases the effective surface area for filtration of oily wastewater. Thereby, enhanced performance in terms of permeation flux is expected. Formation of wrinkles on membranes with GO was also reported in poly(L-lactic acid) membrane coated with GO [44] and polyvinyl alcohol membrane with GO [45]. For membrane with 0.5 phr sulfur content, some micro-cracks or discontinuity could be observed, Figure 1b. This is attributed to low sulfur loading that leads to less crosslink networks which affected continuous strong membrane film formation. At sulfur loading of 1.0 phr, no micro-crack could be observed on the surface of the membrane which suggest the formation of strong and continuous membrane, Figure 1d. The wrinkles and ridges are more apparent at 1.0 phr sulfur loading. In NBR/GO membrane with 1.5 phr sulfur, Figure 1f, less wrinkles and ridges are observed which suggest less migration of GO nanosheets to the surface of the membrane during casting and curing processes. More micro-cracks can also be observed at high magnification which suggest discontinuity on membrane surface.

Phase inversion method is the most common method used to produce porous polymer matrix membrane in which polymer resins are being dissolved in a solvent and casted into films based on phase separation of polymer rich phase from polymer poor phase. In this method, the structural integrity of the membrane is influenced by the solvent type, non-solvent precipitation bath type and precipitation time [46]. However, in the proposed latex compounding and curing method, to produce polymer membrane, the latex membrane integrity and strength is obtained only by sufficient coalescence between latex particle during membrane casting process. Previous studies suggested that an optimum level of latex chains crosslinking inside the latex particle is required to obtain sufficient coalescence between latex particles. Too low or too much crosslinking would retard the extent of coalescence and cause the formation of discontinuous films with micro cracks [47]. Very low crosslinking will cause the particles to aggregate together due to stickiness, while very high crosslinking will cause the particle to become hard and bounces back during coalescence. From the SEM images, it can be concluded that membranes with



good structural integrity without any micro cracks are formed at 1.0 phr sulfur loading. The formation of crosslink is too low and too high at 0.5 and 1.5 phr sulfur loading, respectively. Less wrinkle formation in membranes with 1.5 phr sulfur loading is due to the high crosslink density between the NBR rubber chains, which restricts the mobility of the NBR chains, increases viscosity of the compound and prevents the GO nanosheets from emerging to the surface of the membrane.

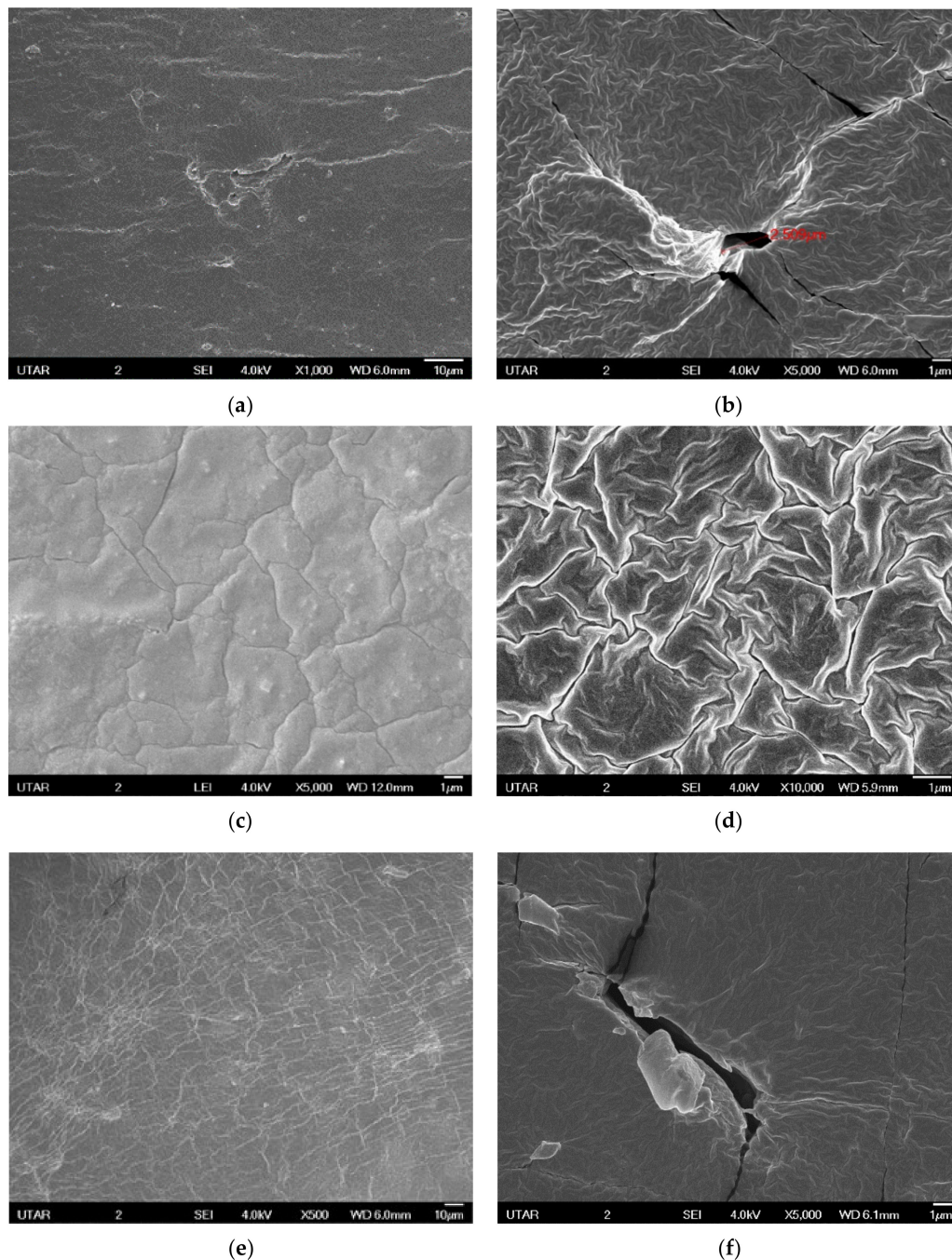


**Figure 1.** SEM micrographs of the membrane surface with different sulfur loadings. (a) 0.5 phr sulfur/0 phr GO, (b) 0.5 phr sulfur/2.0 phr GO, (c) 1.0 phr sulfur/0 phr GO, (c) 1.0 phr sulfur/0 phr GO, (d) 1.0 phr sulfur/ 2.0 phr GO, (e) 1.5 phr sulfur/0 phr GO, (f) 1.5 phr sulfur/2.0 phr GO.

The FTIR spectrums in Figure 2 present the functional groups of NBR latex membranes with and without GO prepared using different loadings of sulfur. The peak around  $3400\text{ cm}^{-1}$  shows the presence of O-H functional group due to surface-adsorbed water

molecules [48]. Peak around  $1560\text{ cm}^{-1}$  represents the N-H bending in NBR. The presence of carboxylic acid O-H stretch can be seen at peak around  $1447\text{ cm}^{-1}$ . Transmission frequencies at  $969\text{ cm}^{-1}$  are due to C-O bending [49]. With respect to sulfur crosslinks, peak readings approximately at  $921$ ,  $721$  and  $538\text{ cm}^{-1}$  indicate the presence of S-OR stretch and S-S disulfide stretch [50]. There are no new peaks other than GO peaks for NBR/GO membranes which indicates there are no new chemical interaction formations between GO and NBR membranes. Thus, the interaction between NBR and GO is purely a physical interaction.

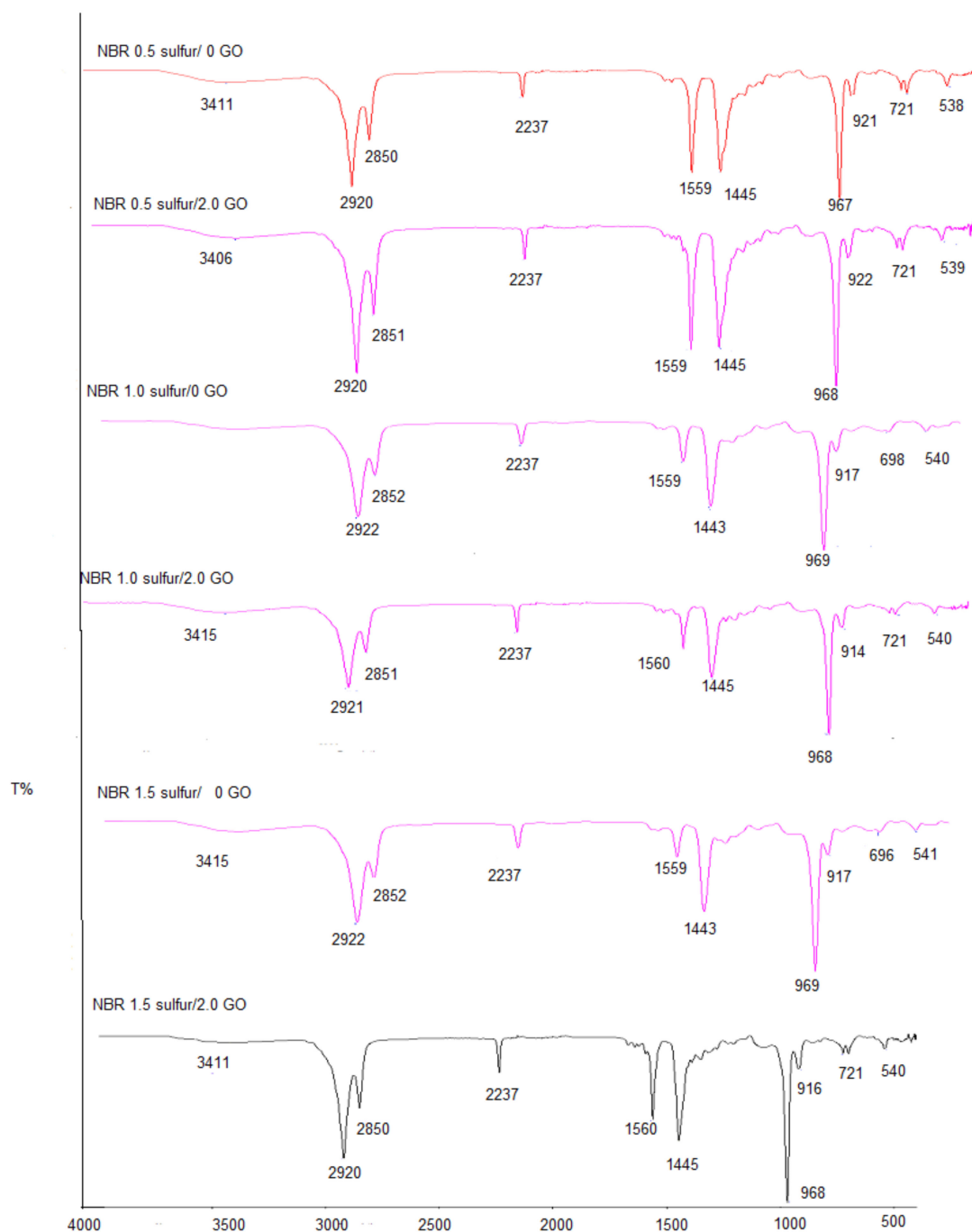


**Figure 2.** FTIR spectra for NBR and NBR/GO membrane.

XRD analysis was carried out to understand the effect of different sulfur loadings on the dispersion of GO nanosheets in NBR latex membrane, Figure 3. A sharp and intense

peak at  $2\theta = 10^\circ\text{--}12^\circ$  is the fingerprint diffraction peak for GO [51]. This peak corresponds to the ordered intercalated structure of GO nanosheets with oxygen functional groups such as epoxide and hydroxyl attached to its basal plane while carboxyl and carbonyl attached to the edges. In average 6–7 graphene layers stack together to form the GO nanostructure. In the XRD diffraction spectrum of the membranes, regardless of the sulfur loading, the sharp intense peak at  $2\theta = 10^\circ\text{--}12^\circ$  has been replaced with broad peak at  $2\theta = 10^\circ\text{--}25^\circ$ , which indicates that the number of GO nanosheets stacking into layers had been reduced. It also indicates the exfoliation of GO nanosheets in the membrane [52].

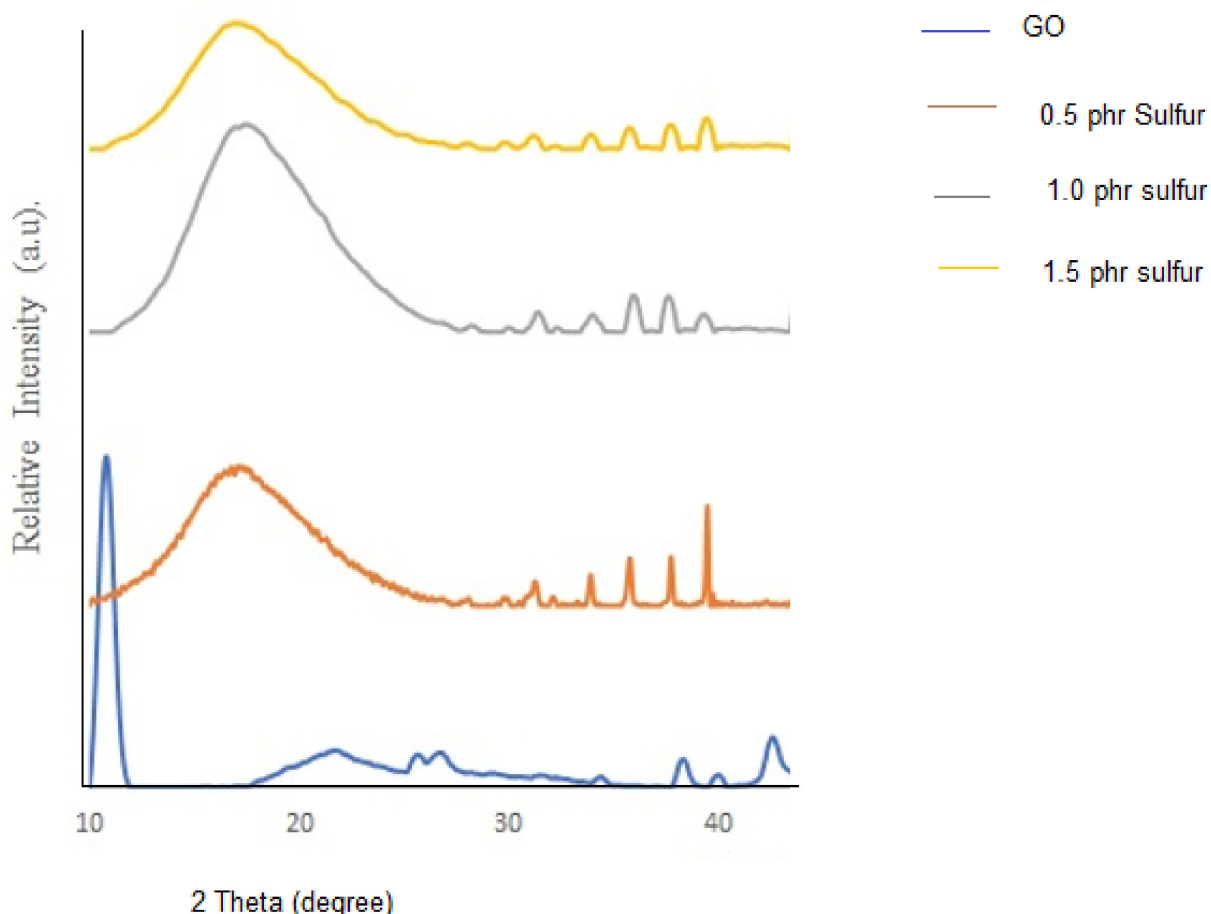


**Figure 3.** XRD pattern of GO and NBR/GO membranes at different sulfur loadings.

### 3.2. Performance Test

#### 3.2.1. Tensile Test

Figures 4–6 exhibit the ultimate tensile strength (UTS), % elongation at break and E-modulus of the membranes with different sulfur loadings. The membrane with GO exhibits higher UTS and E-modulus compared to pure NBR membrane at all sulfur loadings. As evidenced from XRD results, GO dispersion could be observed for all the membranes regardless of sulfur loading. Dispersion of GO will promote good interaction between GO filler and NBR matrix and thus leads to efficient stress transfer between filler and matrix. Moreover, addition of GO as filler greatly improves membrane strength due to its excellent mechanical properties, high surface area and stiffness. The UTS and E-modulus also increase proportionally with the increment in sulfur loading.



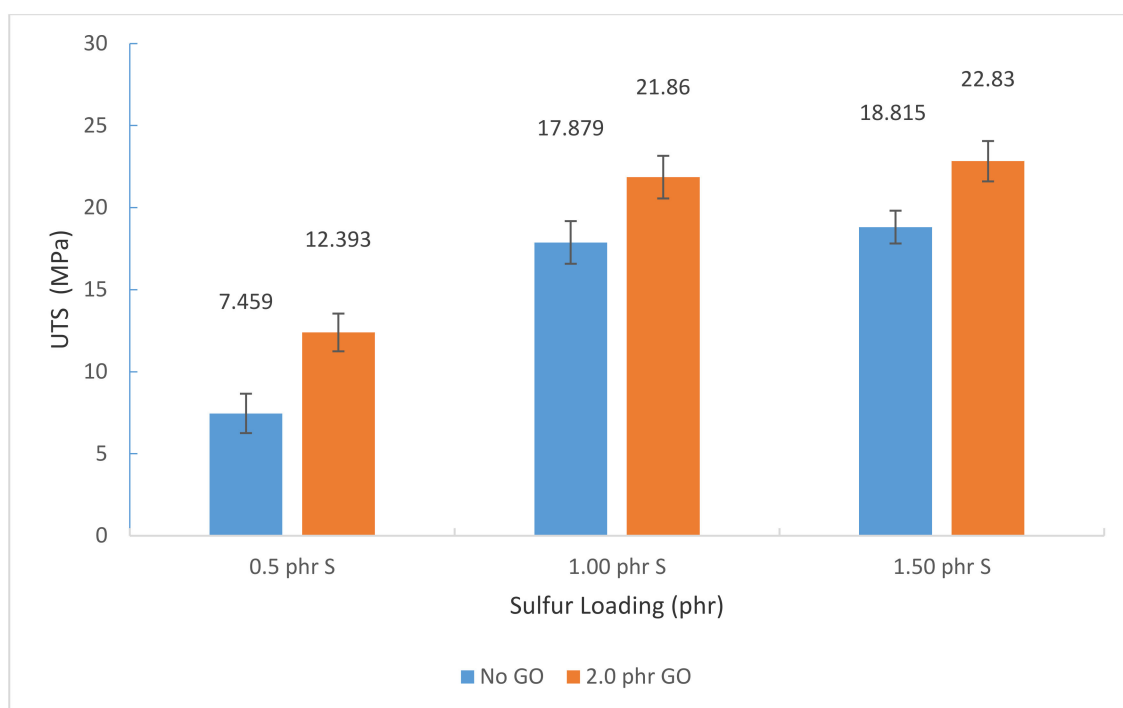


**Figure 4.** Ultimate tensile strength (UTS) of the membranes.

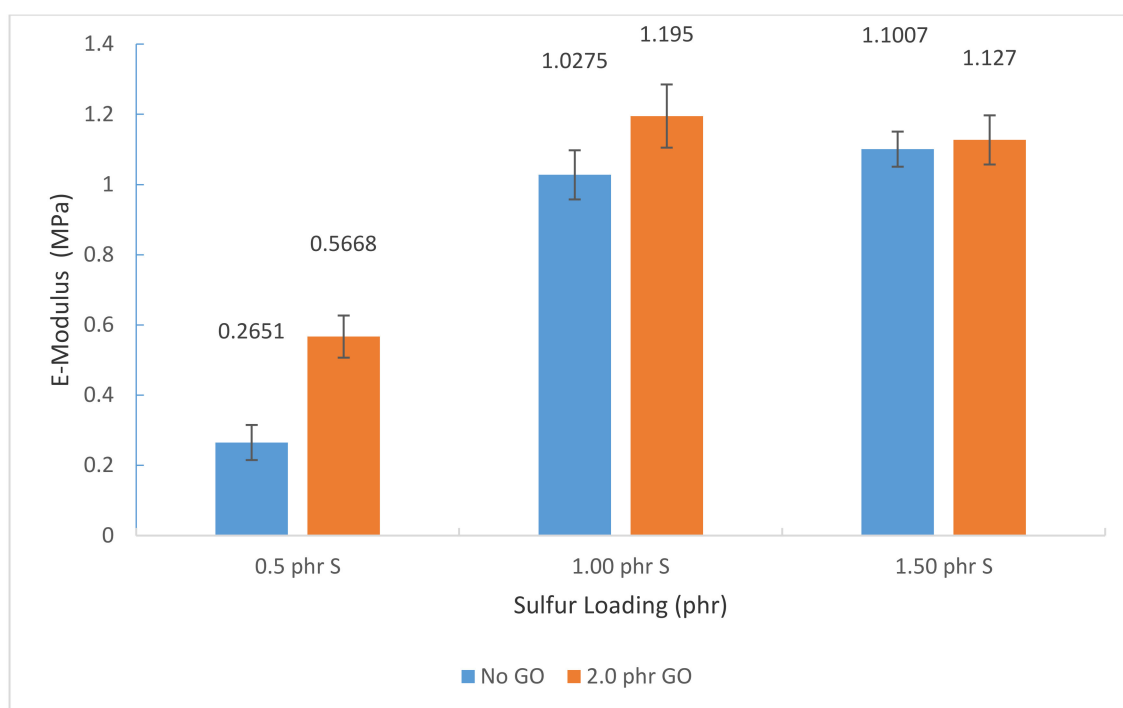


**Figure 5.** E-modulus of the membranes.

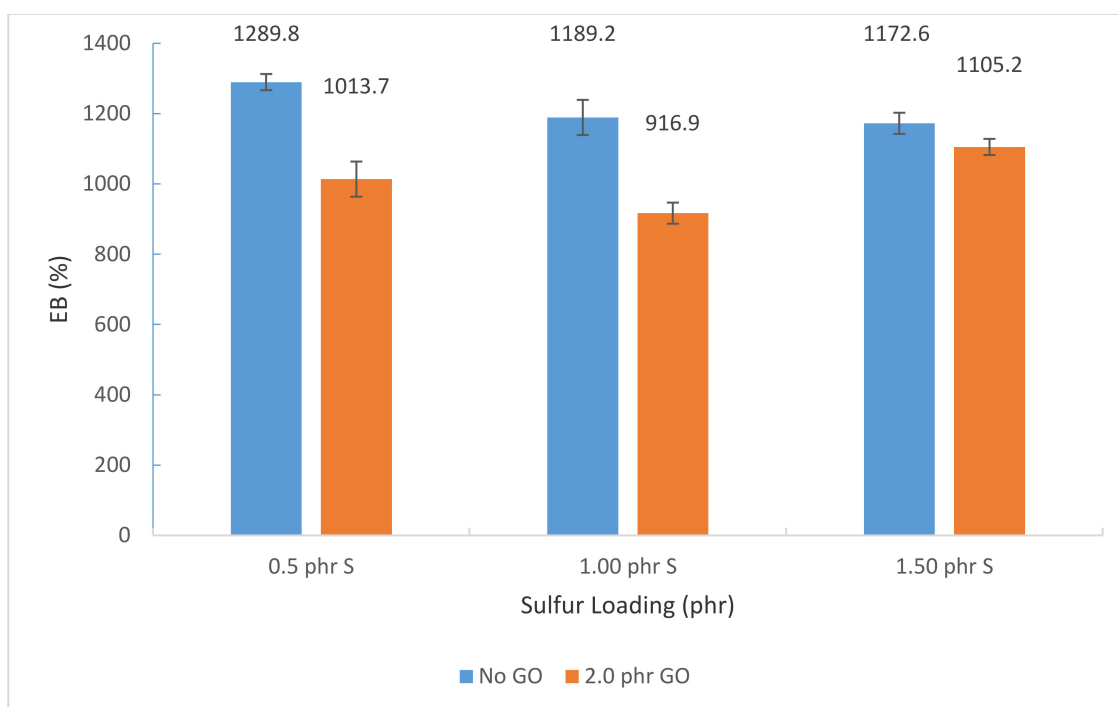


**Figure 6.** Elongation at break of the membrane.

This proportional relationship is due to the crosslink density. According to Linhares et al., the increase in sulfur loading results in higher crosslink density and therefore higher moduli, stiffness, hardness and material strength could be imparted [53]. Preparation of membranes using the latex compounding and curing method has yielded membranes with higher and comparable UTS (21–22 MPa) with polymeric membranes produced through other methods. For instance, polyvinyl chloride (PVC) membrane incorporated with 0.75 wt.% GO shows UTS value of 5.46 MPa [54], polyethersulfone-functionalized GO shows maximum UTS improvement up to 22 MPa [55] and polysulfone (PSF) membrane filled with 0.25% GO shows UTS value of 4.06 MPa [56]. Comparison of UTS with latex-based membrane is not possible because to the best of our knowledge, this research work is the first attempt to produce latex-based membranes. However, the % elongation of the membranes decreases when the sulfur loading increases. As membranes have more crosslinks, the rubber chain mobility will be restricted and the chains are unable to dissipate heat generated by deformation through molecular motion, resulting in easy and brittle rupture at low elongation [57].

### 3.2.2. Permeation Flux Efficiency

Figure 7 shows the permeation flux of membranes with different loadings of sulfur measured at pressures of 0.5 and 1.0 bar in order to study the function of operating pressure on the permeation flux efficiency. It was found that pure NBR membrane with 1.0 and 1.5 phr sulfur did not show any water flux due to the lack of hydrophilicity of the membrane [58]. In pure NBR membrane, there is absence of GO, hence, this leads to absence of hydrophilic property in the membrane. The pure NBR membrane and NBR/GO membrane with 0.5 phr of sulfur content broke or failed during the testing under pressure. As evidenced from the SEM images and UTS results, a continuous and strong membrane was not formed at 0.5 phr sulfur loading. Only NBR/GO membrane with 1.0 and 1.5 phr sulfur loading showed water permeation. GO is hydrophilic in nature; thus, with addition of GO, the overall hydrophilicity of the membrane will increase which then enables the passing of a permeate stream [59]. From Figure 7, the membrane with 1.0 phr of sulfur shows the higher permeation flux of 789.4 and 834.1 L/m<sup>2</sup>·hr at 0.5 and 1.0 bar, respectively, as compared with the membrane with 1.5 phr of sulfur that only shows the permeation

flux of 329.9 and 559.6 L/m<sup>2</sup>·hr. This is because the higher the sulfur loading, the higher the crosslink density that causes the chains between the NBR polymeric system to become more compact. Consequently, the filtration ability of the membrane will reduce. Moreover, the SEM images revealed that wrinkles and ridges in membranes with 1.0 phr sulfur are well formed compared to other membranes. The membrane with 1.5 phr sulfur loading shows less wrinkles and ridges which shows a less effective area for contact with water.

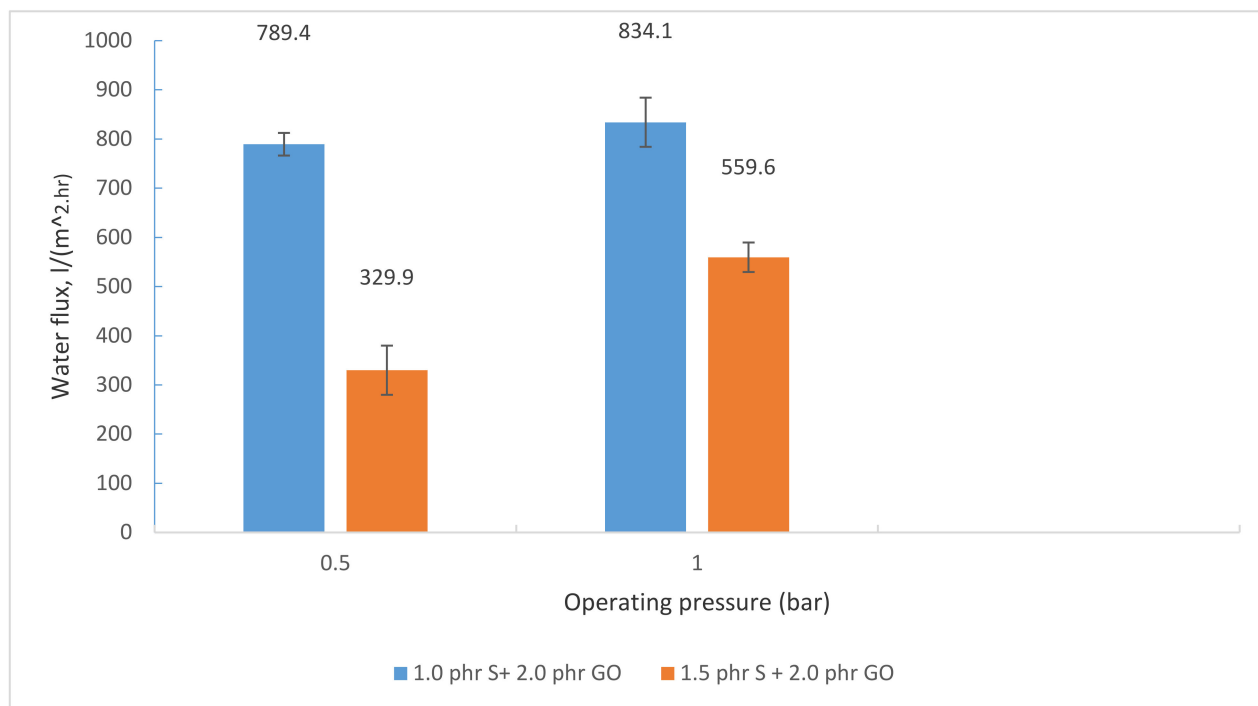


**Figure 7.** Permeation flux of the membrane.

The permeation flux of the membranes for 1.0 to 1.5 phr of sulfur increases as the operating pressure increases. This is because at higher pressure, the water droplets are able to pass through the membrane more readily [14]. As compared to the literature, the permeation flux of NBR/GO membranes achieved in this work is much higher compared to other membranes. For instance, there was only 153.2 Lm<sup>−2</sup>h<sup>−1</sup> permeation flux reported for filtration of oily wastewater by Yang et al. [11] using Kaolin/MnO<sub>2</sub> bi-layer composite dynamic membrane. Besides, the permeation flux of PVC-bentonite membrane and PAN ultrafiltration membrane were reported as only 186 Lm<sup>−2</sup>h<sup>−1</sup> and 96.2 Lm<sup>−2</sup>h<sup>−1</sup>, respectively, for oily wastewater filtration at a pressure of 4 bars [4,16]. Although the permeation flux of the NBR/GO membrane is much higher than that reported in the literature, the ultimate choice will still be based on the oily wastewater rejection rate. The oily wastewater rejection rate is crucial because the regulatory body requirement must be followed before the wastewater is discharged to the water body.

### 3.2.3. Oil Rejection Efficiency

From Figure 8, the oily wastewater rejection rate of both membranes with 1.0 phr and 1.5 phr sulfur increases from 91.67% to 92.23% and 89.2% to 91.46% respectively, as the operating pressure increases. As the pressure increases from 0.5 to 1 bar, oil droplets start to accumulate on the membrane surface and act as a barrier against passage of oil droplets. Increase in oil rejection upon application of pressure was also reported in previous works but the relationship is not proportional [60].

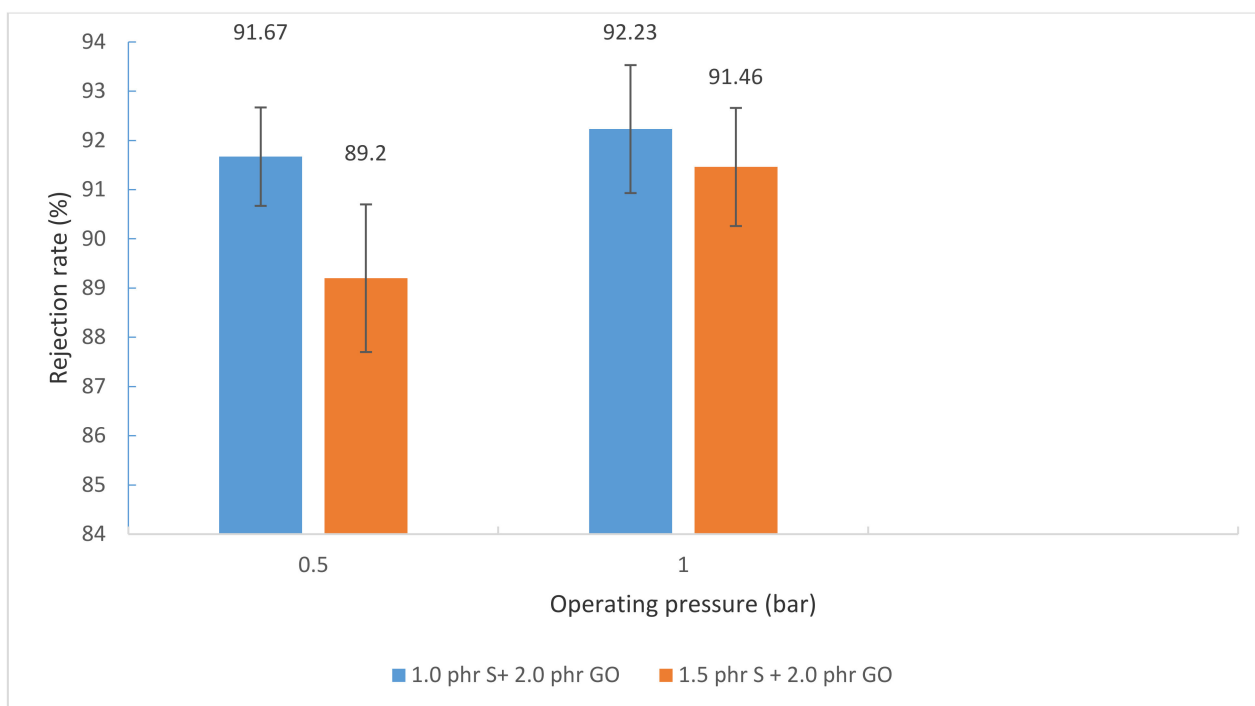


**Figure 8.** Oil rejection rate (%) of the membrane.

The membrane with higher sulfur loading exhibits lower oil rejection efficiency at all pressures. This is due to the cracks found on the surface morphology of the membrane that allows oil particles to seep through the permeate stream to decrease the oil rejection.

In conclusion, oil rejection efficiency of the membrane with 1.0 phr of sulfur is more preferable as compared to the membranes with 0.5 and 1.5 phr of sulfur. Global oil discharge limits in wastewater after treatment have been well-established and the membrane that is expected to be developed needs to achieve the requirement of the global oil discharge limits. According to the environmental regulations that administer the discharge of oily wastewater, the limit on the maximum oil concentration falls generally within 5–100 mg/L [4]. According to the Environmental Protection Agency (EPA) from the United States, the maximum oil concentration of 72 mg/L for any 24 h period is acceptable [60]. Hence, both membranes from this research fulfill the requirement as the discharged oily wastewater through both membranes falls only in the range of 49.57 to 59.90 mg/L in 24 h.

#### 4. Conclusions

In this work, NBR latex/graphene oxide (GO) membranes were successfully fabricated by the latex compounding and curing method. The NBR/GO membrane with 1.0 phr of sulfur exhibits the optimum performance in terms of relatively high permeation flux and high oil rejection efficiency at all pressures. The high permeation flux and high oil rejection efficiency above 90% were the main concern in oily wastewater treatment. This finding was already superior to most of the membranes reported in the literature.

**Author Contributions:** Conceptualization, K.A. and M.K.; methodology, Y.M.; validation, Y.M. and M.K.; formal analysis, Y.T.J. and M.A.; investigation, K.A., Y.T.J., Y.M., and M.K.; resources, K.A.; writing—original draft preparation, Y.T.J., Y.M., and M.K.; supervision, M.K.; project administration, K.A.; funding acquisition, K.A. and M.A. All authors have read and agreed to the published version of the manuscript.

**Funding:** This research was funded by Deputyship for Research& Innovation, Ministry of Education in Saudi Arabia, grant number 32 and “The APC was funded by THE PROJECT INDICATED ABOVE”.

**Institutional Review Board Statement:** Not applicable.

**Informed Consent Statement:** Not applicable.

**Data Availability Statement:** The study did not report any data.

**Acknowledgments:** The authors extend their appreciation to the Deputyship for Research & Innovation, Ministry of Education in Saudi Arabia for funding this research work through the project number 32.

**Conflicts of Interest:** The authors declare no conflict of interest. The funders had no role in the design of the study; in the collection, analyses, or interpretation of data; in the writing of the manuscript, or in the decision to publish the results.

## References

1. Qu, X.; Alvarez, P.; Li, Q. Applications of nanotechnology in water and wastewater treatment. *Water Res.* **2013**, *47*, 3931–3946. [[CrossRef](#)] [[PubMed](#)]
2. Hossein Davood Abadi Farahani, M.; Vatanpour, V.; Hooshang Taheri, A. *Desalination—Challenges and Opportunities, World's Demand for Food and Water: The Consequences of Climate Change*; IntechOpen: London, UK, 2020; Chapter 4. [[CrossRef](#)]
3. Pendergast, M.M.; Hoek, E.M.V. A review of water treatment membrane nanotechnologies. *Energy Environ. Sci.* **2011**, *4*, 1946–1971. [[CrossRef](#)]
4. Tanudjaja, H.J.; Hejase, C.A.; Tarabara, V.V.; Fane, A.G.; Chew, J.W. Membrane-based separation for oily wastewater: A practical perspective. *Water Res.* **2019**, *156*, 347–365. [[CrossRef](#)]
5. Daud, N.M.; Sheikh, A.; Siti, R.; Abu Hasan, H.; Yaakob, Z. Production of biodiesel and its wastewater treatment technologies: A review. *Process Saf. Environ. Prot.* **2015**, *94*, 487–508. [[CrossRef](#)]
6. Yan, L.; Hong, S.; Li, M.L.; Li, Y.S. Application of the Al<sub>2</sub>O<sub>3</sub>—PVDF nanocomposite tubular ultrafiltration (UF) membrane for oily wastewater treatment and its antifouling research. *Sep. Purif. Tech.* **2009**, *66*, 347–352. [[CrossRef](#)]
7. Ahmad, T.; Guria, C.; Mandal, A. A review of oily wastewater treatment using ultrafiltration membrane: A parametric study to enhance the membrane performance. *J. Water Process. Eng.* **2020**, *36*, 101289. [[CrossRef](#)]
8. Zhao, D.; Liu, J.; Qiu, L.; Xu, J.; Jiang, G.; Xue, T.; Wang, B.; Gu, Z.; Liu, G. Roles of a mixed hydrophilic/hydrophobic interface in the regulation of nanofiltration membrane fouling in oily produced wastewater treatment: Performance and interfacial thermodynamic mechanisms. *Sep. Purif. Technol.* **2021**, *257*, 117970. [[CrossRef](#)]
9. Changmai, M.; Pasawan, M.; Purkait, M. Treatment of oily wastewater from drilling site using electrocoagulation followed by microfiltration. *Sep. Purif. Technol.* **2019**, *210*, 463–472. [[CrossRef](#)]
10. Munirasu, S.; Abu Haija, M.; Banat, F. Use of membrane technology for oil field and refinery produced water treatment—A review. *Process Saf. Environ. Prot.* **2016**, *100*, 183–202. [[CrossRef](#)]
11. Chakrabarty, B.; Ghoshal, A.K.; Purkait, M.K. Ultrafiltration of stable oil-in-water emulsion by polysulfone membrane. *J. Membr. Sci.* **2008**, *325*, 427–437. [[CrossRef](#)]
12. Huang, S.; Ras, R.H.; Tian, X. Antifouling membranes for oily wastewater treatment: Interplay between wetting and membrane fouling. *Curr. Opin. Colloid Interface Sci.* **2018**, *36*, 90–109. [[CrossRef](#)]
13. Asatekin, A.; Mayes, A.M. Oil industry wastewater treatment with fouling resistant membranes containing amphiphilic comb copolymer. *Environ. Sci. Technol.* **2009**, *43*, 4487–4492. [[CrossRef](#)]
14. Yang, T.; Ma, Z.; Yang, Q. Formation and characterization of Kaolin/MnO<sub>2</sub> bi-layer composite dynamic membrane for oily wastewater treatment: Effect of solution conditions. *Desalination* **2011**, *270*, 50–56. [[CrossRef](#)]
15. Ahmad, T.; Guria, C.; Mandal, A. Synthesis, characterization and performance studies of mixed-matrix poly(vinyl chloride)-bentonite ultrafiltration membrane for the treatment of saline oily wastewater. *Process. Saf. Environ. Prot.* **2018**, *116*, 703–717. [[CrossRef](#)]
16. Abdolhamid, S.; Ali, G.; Toraj, M.; Sayed Siavash, M. Experimental performance evaluation of polymeric membranes for treatment of an industrial oily wastewater. *Desalination* **2010**, *262*, 235–242.
17. Mittal, P.; Jana, S.; Mohanty, K. Synthesis of low-cost hydrophilic ceramic-polymeric composite membrane for treatment of oily wastewater. *Desalination* **2011**, *282*, 54–62. [[CrossRef](#)]
18. Otitoju, T.; Ahmad, A.; Ooi, B. Polyvinylidene fluoride (PVDF) membrane for oil rejection from oily wastewater: A performance review. *J. Water Process. Eng.* **2016**, *14*, 41–59. [[CrossRef](#)]
19. Daniela, Z.; Igor, C.; Mariana, B.; Militina, B.; Maria, D.; Gabriela, L.; Ionel, M.; Vesna, V.; Jasmina, S. Preparation, characterization and applicability of cellulose acetate–polyurethane blend membrane in separation techniques. *Colloids Surf. A Physicochem. Eng. Asp.* **2010**, *370*, 120–128.
20. Zhang, Z.; Sun, J.; Y Lai, Y.; Wang, Y.; Liu, X.; Shi, S.; Chen, X. Effects of thermal aging on uniaxial ratcheting behavior of vulcanised natural rubber. *Polym. Test.* **2018**, *70*, 102–110. [[CrossRef](#)]
21. Shen, M.; Peng, X.D.; Meng, X.K.; Zheng, J.P.; Zhu, M.H. Fretting wear behavior of acrylonitrile-butadiene rubber (NBR) for mechanical seal applications. *Tribol. Int.* **2016**, *93*, 419–428. [[CrossRef](#)]



22. Zhao, Y.; Yu, W.; Li, R.; Xu, Y.; Liu, Y.; Sun, T.; Shen, L.; Lin, H. Electric field endowing the conductive polyvinylidene fluoride (PVDF)-graphene oxide (GO)-nickel (Ni) membrane with high-efficient performance for dye wastewater treatment. *Appl. Surf. Sci.* **2019**, *483*, 1006–1016. [\[CrossRef\]](#)
23. Lu, J.; Gu, Y.-H.; Chen, Y.; Yan, X.; Guo, Y.-J.; Lang, W.-Z. Ultrahigh permeability of graphene-based membranes by adjusting D-spacing with poly (ethylene imine) for the separation of dye wastewater. *Sep. Purif. Tech.* **2019**, *210*, 737–745. [\[CrossRef\]](#)
24. Zhao, C.; Xu, X.; Chen, J.; Wang, G.; Yang, F. Highly effective antifouling performance of PVDF/graphene oxide composite membrane in membrane bioreactor (MBR) system. *Desalination* **2014**, *340*, 59–66.
25. Wu, W.; Zhang, X.; Qin, L.; Li, X.; Meng, Q.; Shen, C.; Zhang, G. Enhanced MPBR with polyvinylpyrrolidone-graphene oxide/PVDF hollow fiber membrane for efficient ammonia nitrogen wastewater treatment and high-density *Chlorella* cultivation. *Chem. Eng. J.* **2020**, *379*, 122368. [\[CrossRef\]](#)
26. Zhang, Y.; Guo, M.; Pan, G.; Yan, H.; Xu, J.; Shi, Y.; Shi, H.; Liu, Y. Preparation and properties of novel pH-stable TFC membrane based on organic–inorganic hybrid composite materials for nanofiltration. *J. Membr. Sci.* **2015**, *476*, 500–507. [\[CrossRef\]](#)
27. Marjani, A.; Nakhjiri, A.T.; Adimi, M.; Jirandehi, H.F.; Shirazian, S. Effect of graphene oxide on modifying polyethersulfone membrane performance and its application in wastewater treatment. *Sci. Rep.* **2020**, *10*, 1–11. [\[CrossRef\]](#)
28. Rasoul, M.; Javad, K.-S.; Mojtaba, S.-N.; Younes, A. Air gap membrane distillation for enrichment of H<sub>2</sub>18O isotopomers in natural water using poly(vinylidene fluoride) nanofibrous membrane. *Chem. Eng. Process. Process Intensif.* **2016**, *100*, 26–36.
29. Su, C.; Li, Y.; Cao, H.; Lu, C.; Li, Y.; Chang, J.; Duan, F. Novel PTFE hollow fibre membrane fabricated by emulsion electrospinning and sintering for membrane distillation. *J. Memb. Sci.* **2019**, *583*, 200–208. [\[CrossRef\]](#)
30. Bhran, A.; Shoaib, A.; Elsadeq, D.; El-gendi, A.; Abdallah, H. Preparation of PVC/PVP composite polymer membranes via phase inversion process for water treatment purposes. *Chin. J. Chem. Eng.* **2018**, *26*, 715–722. [\[CrossRef\]](#)
31. Liu, H.; Liao, X. The effects of fluorocarbon special surfactant (FS-30) additive on the phase inversion, morphology and separation performance of poly(vinylidene fluoride) (PVDF) membranes. *Sep. Purif. Technol.* **2019**, *212*, 619–631. [\[CrossRef\]](#)
32. Korolkov, I.V.; Gorin, Y.G.; Yeszhanov, A.B.; Kozlovskiy, A.L.; Zdorovets, M.V. Preparation of PET track-etched membranes for membrane distillation by photo-induced graft polymerization. *Mater. Chem. Phys.* **2018**, *205*, 55–63. [\[CrossRef\]](#)
33. Huang, Y.; Huang, Q.L.; Liu, H.; Zhang, C.X.; You, Y.W.; Li, N.N.; Xiao, C.F. Preparation, characterization and applications of electrospun ultrafine fibrous PTFE porous membranes. *J. Memb. Sci.* **2017**, *523*, 317–326. [\[CrossRef\]](#)
34. Naebpetch, W.; Junhasavasdikul, B.; Saetung, A.; Tulyapitak, T.; Nithi-Uthai, N. Influence of filler type and loading on cure characteristics and vulcanisate properties of SBR compounds with a novel mixed vulcanisation system. *Plast. Rubber Compos.* **2017**, *48*, 1–9. [\[CrossRef\]](#)
35. Yew, G.Y.; Tham, T.C.; Law, C.L.; Chu, D.-T.; Ogino, C.; Show, P.L. Emerging crosslinking techniques for glove manufacturers with improved nitrile glove properties and reduced allergic risks. *Mater. Today Commun.* **2019**, *19*, 39–50. [\[CrossRef\]](#)
36. Bhadrar, B.; Vijayan, D.; George, N.; Chandra, C.J.; Begum, P.S.; Joseph, R. Reinforcing effect of organoclay in nitrile rubber-effect of mill mixing and latex stage mixing. *Appl. Clay Sci.* **2018**, *165*, 91–102. [\[CrossRef\]](#)
37. Bakhshandeh, G.R.; Farahani, T.D.; Emamikia, M. Effect of Curing System on Mechanical Properties of NBR / Nylon-PET Cord Composite. *E-Polymers* **2008**, *8*, 273–284. [\[CrossRef\]](#)
38. Hait, S.; Valentin, J.L.; Jimenez, A.G.; Ortega, P.B.; Ghosh, A.K.; Stockelhuber, K.W.; Wiebner, S.; Heinrich, G.; Das, A. Poly (acrylonitrile-co-butadiene) as polymeric crosslinking accelerator for sulphur network formation. *Heliyon* **2020**, *6*, e04659. [\[CrossRef\]](#)
39. Wręczycki, J.; Bieliński, D.; Anyszka, R. Sulfur/Organic Copolymers as Curing Agents for Rubber. *Polymers* **2018**, *10*, 870. [\[CrossRef\]](#)
40. Karzov, I.; Nashchokin, A.; Tikhonov, N.; Kalugin, D.; Malakho, A. Data on compressibility of NBR samples with various cross-linking degree and zinc oxide content immersed in gasoline and oil. *Data Brief* **2020**, *30*, 105470. [\[CrossRef\]](#) [\[PubMed\]](#)
41. Thebo, K.H.; Qian, X.; Zhang, Q.; Chen, L.; Cheng, H.M.; Ren, W. Highly stable graphene-oxide-based membranes with superior permeability. *Nat. Commun.* **2018**, *9*, 1486. [\[CrossRef\]](#) [\[PubMed\]](#)
42. Mensah, B.; Kim, S.; Arepalli, S.; Nah, C. A study of graphene oxide-reinforced rubber nanocomposite. *J. App. Polym. Sci.* **2014**, *131*, 1–9. [\[CrossRef\]](#)
43. Zhong, Y.; Mahmud, S.; He, Z.; Yang, Y.; Zhang, Z.; Guo, F.; Chen, Z.; Xiong, Z.; Zhao, Y. Graphene oxide modified membrane for highly efficient wastewater treatment by dynamic combination of nanofiltration and catalysis. *J. Hazard. Mater.* **2020**, *397*, 122774. [\[CrossRef\]](#)
44. Dave, H.K.; Nath, K. Graphene oxide incorporated novel polyvinyl alcohol composite membrane for pervaporative recovery of acetic acid from vinegar wastewater. *J. Water Process. Eng.* **2016**, *14*, 124–134. [\[CrossRef\]](#)
45. Basile, A.; Mozia, S.; Molinari, R. (Eds.) *Current Trends and Future Developments on (Bio-) Membranes: Photocatalytic Membranes and Photocatalytic Membrane Reactors*; Elsevier: Amsterdam, The Netherlands, 2018.
46. Lee, D.I. The effects of latex coalescence and interfacial crosslinking on the mechanical properties of latex films. *Polymer* **2005**, *46*, 1287–1293. [\[CrossRef\]](#)
47. Du, J.; Wu, Q.; Zhong, S.; Gu, X.; Liu, J.; Guo, H.; Zhang, W.; Peng, H.-L.; Zou, J. Effect of hydroxyl groups on hydrophilic and photocatalytic activities of rare earth doped titanium dioxide thin films. *J. Rare Earths* **2015**, *33*, 148–153. [\[CrossRef\]](#)

48. OChemOnline, November 2014. "Infrared Spectroscopy Absorption Table" Electronic Reference. Available online: [https://chem.libretexts.org/Reference/Reference\\_Tables/Spectroscopic\\_Parameters/Infrared\\_Spectroscopy\\_Absorption\\_Table#title](https://chem.libretexts.org/Reference/Reference_Tables/Spectroscopic_Parameters/Infrared_Spectroscopy_Absorption_Table#title) (accessed on 23 August 2018).
49. Vinayan, B.P.; Zhao-Karger, Z.; Diemant, T.; Chakravadhanula, V.S.K.; Schwarzbürger, N.I.; Cambaz, M.A.; Behm, R.J.; Kübel, C.; Fichtner, M. Performance study of magnesium–sulfur battery using a graphene based sulfur composite cathode electrode and a non-nucleophilic Mg electrolyte. *Nanoscale* **2015**, *8*, 3296–3306. [[CrossRef](#)]
50. Stobinski, L.; Lesiak, B.; Malolepszy, A.; Mazurkiewicz, M.; Mierzwa, B.; Zemek, J.; Jiricek, P.; Bieloshapka, I. Graphene oxide and reduced graphene oxide studied by the XRD, TEM and electron spectroscopy methods. *J. Electron Spectrosc. Relat. Phenom.* **2014**, *195*, 145–154. [[CrossRef](#)]
51. Yang, Z.; Yuan, Z.; Shang, Z.; Ye, S. Multi-functional membrane based on montmorillonite/graphene oxide nanocomposites with high actuating performance and wastewater purification. *Appl. Clay Sci.* **2020**, *197*, 105781. [[CrossRef](#)]
52. Linhares, F.N.; Kersch, M.; Niebergall, U.; Leite, M.C.A.M.; Altstädt, V.; Furtado, C.R.G. Effect of different Sulphur-based crosslink network on the nitrile rubber resistance to biodiesel. *Fuel* **2017**, *191*, 130–139. [[CrossRef](#)]
53. Namdar, H.; Akbari, A.; Yegani, R.; Roghani-Mamaqani, H. Influence of aspartic acid functionalized graphene oxide presence in polyvinylchloride mixed matrix membranes on chromium removal from aqueous feed containing humic acid. *J. Environ. Chem. Eng.* **2021**, *9*, 104685. [[CrossRef](#)]
54. Giwa, A.; Hasan, S.W. Novel polyethersulfone-functionalized graphene oxide (PES-fGO) mixed matrix membranes for wastewater treatment. *Sep. Purif. Technol.* **2020**, *241*, 116735. [[CrossRef](#)]
55. Ammar, A.; Al-Enizi, A.M.; AlMaadeed, M.A.; Karim, A. Influence of graphene oxide on mechanical, morphological, barrier, and electrical properties of polymer membranes. *Arab. J. Chem.* **2016**, *9*, 274–286. [[CrossRef](#)]
56. Mok, K.L.; Eng, A.H. Characterisation of crosslinks in vulcanized rubbers: From simple to advanced techniques. *Malays. J. Chem.* **2017**, *20*, 118–127.
57. Thomas, S.P.; Thomas, S.; Marykutty, C.V.; Mathew, E.J. Evaluation of effect of various nanofillers on technological properties of NBR/NR blend vulcanized using BIAT-CBS system. *J. Polym.* **2013**, *2013*, 1–10. [[CrossRef](#)]
58. Zhang, X.; Fan, X.; Li, H.; Yan, C. Facile preparation route for graphene oxide reinforced polyamide 6 composites via in situ anionic ring-opening polymerization. *J. Mater. Chem.* **2012**, *22*, 24081–24091. [[CrossRef](#)]
59. Gorouhi, E.; Sadrzadeh, M.; Mohammadi, T. Microfiltration of oily wastewater using PP hydrophobic membrane. *Desalination* **2006**, *200*, 319–321. [[CrossRef](#)]
60. Chen, A.S.C.; Flynn, J.T.; Cook, R.G.; Casaday, A.L. Casaday Removal of oil, grease, and suspended solids from produced water with ceramic crossflow microfiltration. *SPE Prod. Eng.* **1991**, *6*, 131–136. [[CrossRef](#)]